Letter

Abnormal scaling of the anomalous Hall effect in noncollinear antiferromagnetic metals from two-center scattering

Lei Wang [1,*] Tai Min,[1] and Ke Xia[2,†]

[1]*Center for Spintronics and Quantum Systems, State Key Laboratory for Mechanical Behavior of Materials, Xi'an Jiaotong University, No. 28 Xianning West Road Xi'an, Shaanxi 710049, China*

[2]*School of Physics, Southeast University, Nanjing 211189, China*

(Received 6 December 2022; revised 27 May 2023; accepted 6 June 2023; published 13 June 2023)

The anomalous Hall effect is generally treated to originate from the Berry curvature of the band structure and scattering of the impurities, which is mainly attributed to the skew scattering and side jump for a single scattering source. In this Letter, using a first-principles-based scattering wave-function approach, we find an abnormal scaling law of the anomalous Hall effect in $L1_2$-type Mn_3X (X = Ir, Pt, Rh). Different from current conventional skew scattering, side jump, and Berry curvature contributions, this abnormal scaling law is demonstrated to come from a two-center scattering (TCS) contribution. Moreover, the corresponding anomalous Hall conductivity can be as large as $\sigma^{\mathrm{H}} \simeq 5 \times 10^4$ $(\Omega\,\mathrm{cm})^{-1}$ in $L1_2$-type Mn_3Ir at low temperature, which is two orders of magnitude larger than the current Berry curvature calculations, indicating that the TCS contribution dominates the anomalous Hall effect in noncollinear antiferromagnetic metals.

DOI: 10.1103/PhysRevB.107.L220402

The anomalous Hall effect refers to the generation of a transverse charge current by an electrical current flowing in a ferromagnetic conductor [1–9], which is one of the most important topics in the field of spintronics and could be extensively applied in devices [10–17]. Generally, the anomalous Hall effect is attributed to two contributions, the Berry curvature from the band structure and the scattering of impurities, and the universal scaling law of the anomalous Hall effect can be written as [12]

$$-\sigma^{\mathrm{H}} = c + \sum_i c_i \rho_i/\rho_{zz} + \left(\sum_{ij} c_{ij}\rho_i\rho_j + \sum_{i\in\mathcal{S}} \alpha_i \rho_i\right)\Big/ \rho_{zz}^2, \tag{1}$$

where c represents the Berry curvature contribution, c_i and c_{ii} are from the side jump contributions of the ith impurity, ρ_i is the resistivity induced by the ith impurity, and $\rho_{zz} = \sum_i \rho_i$, accordingly. α denotes the skew scattering contribution. Here, it should be noted that the scattering is strongly dependent on the type of impurities, such as the dynamic impurity with a Gaussian-like impurity potential and static impurity from element doping. For example, because the skew scattering is proportional to the third power of the impurity potential [18], only the static impurities contribute to the skew scattering, and the corresponding configuration average of the dynamic impurities vanishes the skew scattering. Thus, $\mathcal{S}$ stands for the group of static impurities, accordingly. Then, there could be different kinds of scaling laws for given systems, e.g., a constant $-\sigma^{\mathrm{H}} = c$ for a pure clean system, a linear $-\sigma^{\mathrm{H}} = \alpha_0\sigma_{zz} + (c + c_0 + c_{00})$ for a single static impurity, and a constant $-\sigma^{\mathrm{H}} = c + c_0 + c_{00}$ for a single dynamic impurity.

Here, we should notice that, for conventional ferromagnetic materials, the scattering contributions are mainly attributed to the skew scattering and side jump from a single scattering source [19–21], where the spin-orbit coupling and spin splitting locate at the same atom. However, for antiferromagnetic materials, e.g., Mn_3X (X = Ir, Pt, Rh), the centers of the spin-orbit coupling and the spin splitting are separated into X and Mn atoms, respectively. Thus, following Eq. (1), when introducing disorders on Ir and Mn atoms, the corresponding two-center scattering (TCS) may induce a new contribution (c_{ij} with $i \neq j$) to the anomalous Hall effect and a different scaling law accordingly. However, even though this TCS contribution is proposed implicitly in Eq. (1), this part of the contribution has received little attention and has been drowned out by the conventional contributions in ferromagnetic metals.

Moreover, in recent decades, along with increasing interest in antiferromagnetic materials due to their intrinsic advantages of robustness against external magnetic fields, no stray fields, and ultrafast dynamics [22–24], many intriguing spin-related phenomena therein and potential applications using antiferromagnetic materials have become the center of attention, including the anomalous Hall effect [25–36]. Even so, for noncollinear antiferromagnetic materials, most of the theoretical work focuses on the Berry curvature contribution [25,26,28,30] and neglects the contributions of the scattering process. However, the experimental results report the temperature, thicknesses, and size dependency of the anomalous Hall effect [29,32,34–39], delivering the information that the scattering process should be even more important.

All of the above knowledge inspires us to carry out the first-principles method with impurity scattering to reveal the fundamental physical mechanism of the anomalous Hall effect in noncollinear antiferromagnetic materials. In this Letter, we mainly chose $L1_2$-type Mn_3Ir (see the crystal structure and magnetic texture in Fig. 1) as an object of this study, and

*wanglei.icer@xjtu.edu.cn
†kexia@seu.edu.cn

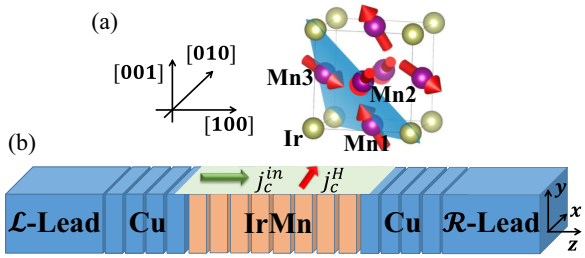

FIG. 1. The sketch of the calculated system. (a) The crystal structure and magnetic texture of $L1_2$-type Mn_3Ir, where Ir locates at the vertex of the fcc lattice, and three Mn atoms locate at the corresponding nonequivalent face centers with a triangle spin configuration inside the [111] plane. (b) The devicelike transport system with two Cu leads sandwiching one Mn_3Ir thin film and the diagram of the injecting charge currents ($j_c^{\rm in}$) and the corresponding Hall current $j_c^{\rm H}$.

find a giant anomalous Hall conductivity therein, which is two orders of magnitude larger than the results from Berry curvature calculations. Moreover, with a detailed analysis of the scaling law, we conclude that this extraordinary anomalous Hall effect is dominated by the TCS contribution. To check the generality of this effect, we also carry out anomalous Hall effect calculations in Mn_3Pt and Mn_3Rh with similar structures, and all the results are mutually corroborated.

In detail, for a transport system with lateral ($x-y$ plane) periodic boundary conditions as shown in Fig. 1(b), the local charge current density from atom R' to atom R is calculated by an exact muffin-tin orbital (EMTO)-based transport code [14,31], which uses the Ando method [40] implemented with EMTOs [14,41–44] and the current operators are the same to the previous MTO-based methods [14,31,44–50], which reads

$$\mathbf{j}_c(\mathbf{R},\mathbf{R}') = 2(\mathbf{R}-\mathbf{R}')\mathrm{Im}\langle\Psi_R|\hat{\mathcal{H}}_{\mathbf{RR}'}|\Psi_{R'}\rangle/\hbar, \qquad (2)$$

where $|\Psi_R\rangle$ is the scattering wave functions [40,45,46] on site R and $\hat{\mathcal{H}}_{\mathbf{RR}'}$ is the corresponding hopping Hamiltonian between atom R and R'. Thus, by projecting $\mathbf{j}_c$ to the longitudinal and transverse directions, we obtain the injected charge current $j_c^{\rm in}$ and the corresponding anomalous Hall current $j_c^{\rm H}$, respectively. Then the anomalous Hall angles are given by $\Theta = j_c^{\rm H}/j_c^{\rm in}$ and the anomalous Hall conductivity by $\sigma^{\rm H} = \Theta/\rho_{zz}$ with ρ_{zz} the longitudinal resistivity.

To study the anomalous Hall effect with impurities, we set up a scattering geometry as shown in Fig. 1(b), which consists of two crystalline semi-infinite Cu leads sandwiching a scattering region of $L1_2$-type Mn_3Ir, in which we can introduce phonon contributions by randomly adding atomic displacements on the equilibrium atom position [14,31,49,51–53], which is constructed by a standard Gaussian distribution with a temperature-dependent root mean square (Δ) estimated by the Debye model [51,52]. Considering that the Debye temperature for Mn_3Ir is about $\theta_D = 400$ K [54], the corresponding root mean square at room temperature ($T = 300$ K) is about $\Delta/a_{\rm Mn_3Ir} \simeq 0.030$, where $a_{\rm Mn_3Ir}$ is the lattice constant of $L1_2$-type Mn_3Ir. Then we first focus on the anomalous Hall effect in $L1_2$-type Mn_3Ir at low temperature ($\Delta/a_{\rm Mn_3Ir} < 0.021$) by neglecting the magnon contributions for a clear view of the physical picture and introduce random magnetic fluctuations to qualitative study the contribution of the magnon. In this

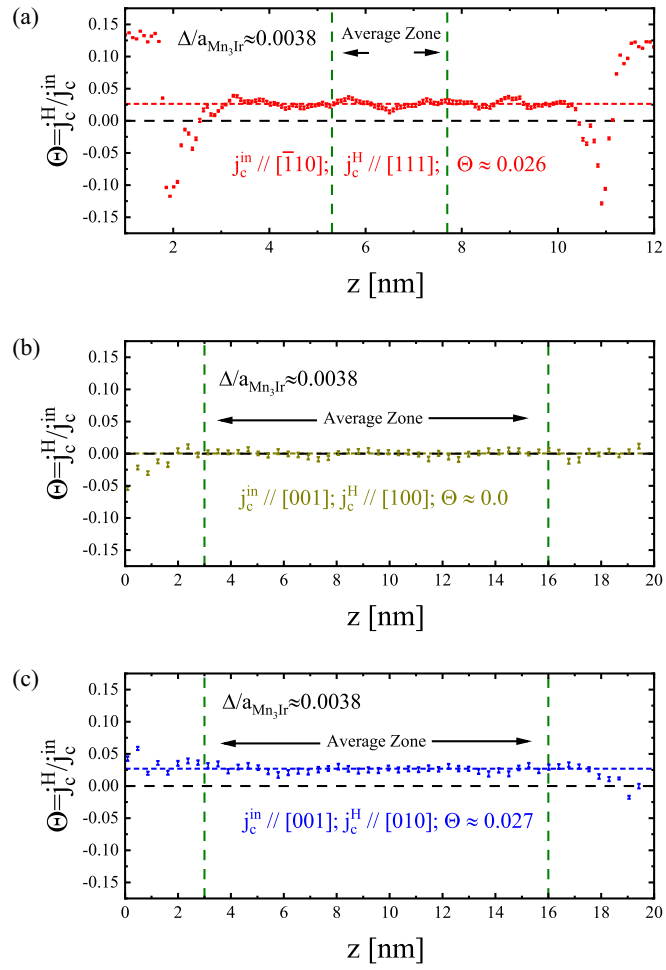

FIG. 2. The anomalous Hall angles (Θ) of Mn_3Ir vs the longitudinal coordinates (z) for different crystal orientations. Here, we only show the results with a finite root mean square $\Delta/a_{\rm Mn_3Ir} \simeq 0.0038$, where $a_{\rm Mn_3Ir}$ stands for the lattice constant of Mn_3Ir. The dashed green lines identify the "average zone" for the bulk value of the anomalous Hall angles.

Letter, we study the anomalous Hall effect by injecting charge current in different crystal orientations ([$\bar{1}$10] and [001]) of the fcc lattice as shown in Fig. 1(a) and calculated the corresponding Hall current in [111], [100], and [010], respectively. To make the results converge, we use 20–30 configurations of random disorder for different cases.

The calculated anomalous Hall angles for a finite $\Delta/a_{\rm Mn_3Ir} \simeq 0.0038$ as a function of the longitudinal coordinates (z) are plotted in Fig. 2 for different crystal orientations. Except for the changes near the interfaces between the Cu leads and Mn_3Ir, all values fluctuate around a finite number. Thus, to avoid the influence of the interfaces and obtain the anomalous Hall angle of the bulk Mn_3Ir, we only average the values inside the "average zone" as shown by the dashed green lines in Fig. 2. Here, one should notice that the anomalous Hall angles for different crystal orientations are different, which agrees with the previous prediction of the anisotropic anomalous Hall effect [26]. However, as the longitudinal resistivity for the case in Fig. 2(c) is only about $\rho_{zz} \simeq 0.54$ μΩ cm, the anomalous conductivity can be obtained as

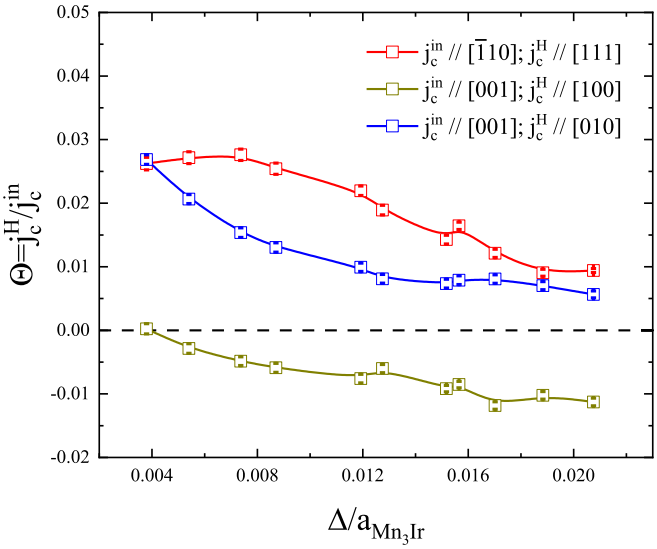

FIG. 3. The anomalous Hall angles (Θ) of Mn_3Ir as a function of the root mean square (Δ) for different crystal orientations.

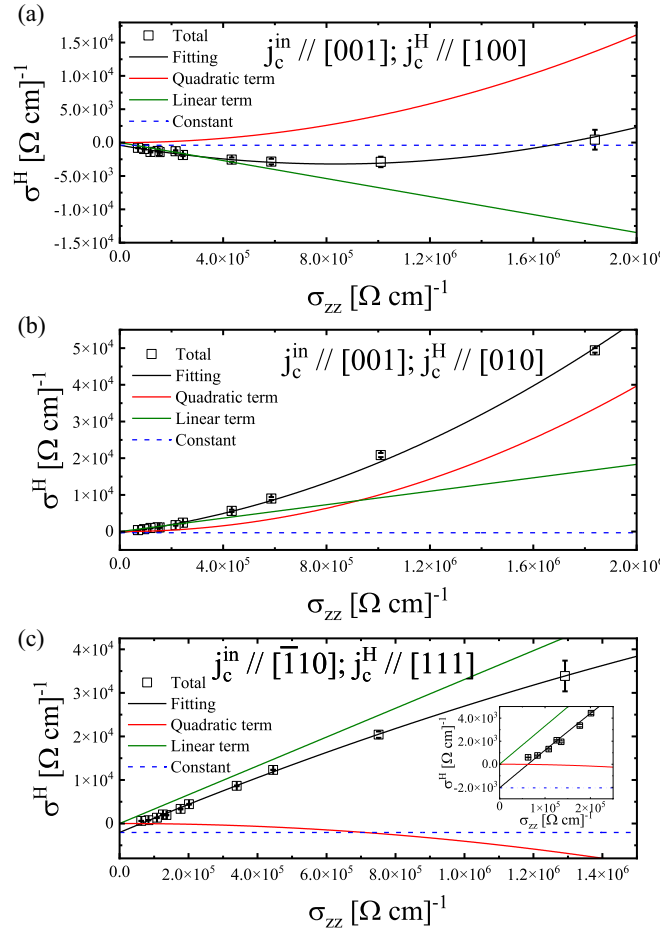

FIG. 4. The anomalous Hall conductivity (σ^{H}) vs the longitudinal conductivity σ_{zz} of Mn_3Ir for different crystal orientations. The black solid lines are the fitting curves using Eq. (3), with all three terms shown by red, green, and blue lines, respectively. The inset of (c) shows the enlarged image.

$\sigma^{\mathrm{H}} \simeq \Theta/\rho_{zz} \simeq 5 \times 10^4\ (\Omega\,\mathrm{cm})^{-1}$. This value is two orders of magnitude larger than the Berry curvature calculations, which are 218 $(\Omega\,\mathrm{cm})^{-1}$ [25] and 312 $(\Omega\,\mathrm{cm})^{-1}$ [26] from different groups, indicating that the Berry curvature from the band structure is not enough for the anomalous Hall effect in Mn_3Ir at finite temperature.

More detailed calculations of the anomalous Hall angles (Θ) for various Δ are plotted in Fig. 3, where Θ decreases when increasing Δ for all three cases. These tendencies differ from our previous results in conventional ferromagnetic metals [14], indicating a totally different scaling law. Therefore, we reorganize our data into the relation between σ^{H} and $\sigma_{zz} = 1/\rho_{zz}$ for a clear view of the scaling law, as shown in Fig. 4.

Before going deep into the data analysis, we first try to simplify Eq. (1) by our specific case of disorders. In our calculations, the phonon is introduced by random atomic displacement of both Ir and Mn atoms, thus the transport electrons will be scattered by the atomic displacement of both Ir and Mn atoms, respectively. As the spin-orbit coupling is mainly from the Ir atom and the spin splitting is mainly from the Mn atom, there will be two types of scattering centers (spin-orbit coupling center at Ir and spin-splitting center at Mn) for the anomalous Hall effect. Therefore, the total resistivity can be separated as $\rho_{zz} = \rho_0 + \rho_1$, with ρ_0 and ρ_1 representing the contributions from the electron scattering by the atomic displacement of Ir and Mn atoms, respectively. Moreover, as reported [18], the skew scattering is proportional to the third power of the impurity potential, and the corresponding configuration average of atomic displacement will vanish the skew scattering contribution accordingly. Then, we have $\mathcal{S} = \emptyset$ and Eq. (1) can be rewritten as

$$-\sigma^{\mathrm{H}} = k_2\sigma_{zz}^2 + k_1\sigma_{zz} + k_0, \tag{3}$$

where $k_0 = c + c_1 + c_{11}$, $k_1 = (c_0 - c_1 - 2c_{11} + 2c_{01})\rho_0$, and $k_2 = (c_{00} + c_{11} - 2c_{01})\rho_0^2$. Furthermore, the Ir atoms cannot generate an anomalous Hall effect itself, thus, $c_0 = c_{00} = 0$, then $k_1 = (-c_1 - 2c_{11} + 2c_{01})\rho_0$ and $k_2 = (c_{11} - 2c_{01})\rho_0^2$. We should notice that k_1 and k_2 are independent of the Berry curvature contribution, and k_0 contains both the side jump and Berry curvature contributions. Under these considerations, the parameters can be fitted out for all three cases in Fig. 4.

Let us first look into the simplest case in Fig. 4(a), where the curve agrees with a simple quadratic polynomial, and the fitting parameters are $k_2/(\mu\Omega\,\mathrm{cm})^2 \simeq -(4.0 \pm 1.0) \times 10^3\ (\Omega\,\mathrm{cm})^{-1}$, $k_1/(\mu\Omega\,\mathrm{cm}) \simeq (7 \pm 1) \times 10^3\ (\Omega\,\mathrm{cm})^{-1}$, and $k_0 \simeq 395 \pm 115\ (\Omega\,\mathrm{cm})^{-1}$. Here, we normalize the units of $k_{1,2}$ by the unit of ρ_0 for a better comparison between each component. Similarly for the case in Fig. 4(b), the parameters can be obtained as $k_2/(\mu\Omega\,\mathrm{cm})^2 \simeq -(9.9 \pm 0.7) \times 10^3\ (\Omega\,\mathrm{cm})^{-1}$, $k_1/(\mu\Omega\,\mathrm{cm}) \simeq -(9 \pm 1) \times 10^3\ (\Omega\,\mathrm{cm})^{-1}$, and $k_0 \simeq 323 \pm 105\ (\Omega\,\mathrm{cm})^{-1}$. The two obtained k_0's are close to each other and quite similar to the Berry curvature results, which are 218 $(\Omega\,\mathrm{cm})^{-1}$ [25] and 312 $(\Omega\,\mathrm{cm})^{-1}$ [26], respectively. As k_0 contains the contributions from both the Berry curvature and side jump, we can conclude that the side jump contribution (c_1 and c_{11}) should be in the same order as the Berry curvature and much smaller than

the total anomalous Hall conductivity in Mn_3Ir. For Fig. 4(c), we still obtain a good fitting curve as shown by the solid black line therein. But interestingly, we have a relatively smaller $k_2/(\mu\Omega\,\mathrm{cm})^2 \simeq (4.1 \pm 0.8) \times 10^3\ (\Omega\,\mathrm{cm})^{-1}$ and a much larger $k_1/(\mu\Omega\,\mathrm{cm}) \simeq -(3.3 \pm 0.1) \times 10^4\ (\Omega\,\mathrm{cm})^{-1}$, together with $k_0 \simeq (2.1 \pm 0.2) \times 10^3\ (\Omega\,\mathrm{cm})^{-1}$, respectively. Thus, the pure scattering process k_1 dominates the anomalous Hall effect in Mn_3Ir as shown in Fig. 4(c) by the green solid line. Summarizing all the above information, we conclude that (1) $k_1/\rho_0 = -c_1 - 2c_{11} + 2c_{01}$ dominates, and (2) $k_0 = c + c_1 + c_{11}$ from the Berry curvature and side jump contributions are much smaller, thus the TCS (c_{01}) should be the key to this giant anomalous Hall effect, and it shows a strong anisotropic effect for different transport directions.

The aforementioned outcome has prompted us to reevaluate this phenomenon from TCS, where the electrons are scattered by two types of scattering centers within the transport scattering time. In this sense, the distance between the scattering centers should be important for this effect. Considering that the conventional linear scaling law expires when the concentration of the impurities is larger than 1% [14], the TCS will be non-negligible when the distance between impurities is smaller than 1.3 nm. Thus, the TCS could be stronger in Mn_3Ir due to the distance between the atomic displacements of Ir and Mn atoms is only about 0.27 nm.

The calculations for Mn_3X with X = Pt, Rh, and $Pt_{1-c}Ir_c$ are also carried out to check the generality of the giant anomalous Hall effect and the calculated results are plotted in Fig. 5, where the giant anomalous Hall effect still exists in Mn_3Pt and Mn_3Rh. Here, one should notice that, as shown in Fig. 5(a), the anomalous Hall angle of Mn_3Pt is quite close to that of Mn_3Ir, but the anomalous Hall angle of Mn_3Rh is smaller. Additionally, an artificial Mn_3Cu with the same structure is introduced to check the contribution of the spin-orbit coupling strength of atom X, where, as shown in Fig. 5(a), the anomalous Hall angle of Mn_3Cu is almost zero. Combining with the previous discussion of Fig. 4 and Eq. (3), we can conclude that both the disorder and spin-orbit coupling strength of the atom X in Mn_3X are important for this giant anomalous Hall effect. Thus, ρ_0 in Eq. (3) can be attributed to the spin-orbit scattering as reported previously [55].

We also generate magnetic fluctuation in Mn_3Pt by randomly rotating the magnetization with a small angle $\delta\theta$ within the Gaussian distribution (only positive values) and a uniform distribution in the range of $[0, 2\pi]$. Typically, we set $\langle\delta\theta\rangle \simeq 3^\circ$ for low temperature, and the results are plotted in Fig. 5 by violet hexagons. It can be seen that the Θ slightly decreases, while ρ_{zz} increases a lot, ending up with a decrease of σ^{H}, even though the anomalous Hall conductivity still has a giant value of $\sim 1.5 \times 10^4\ (\Omega\,\mathrm{cm})^{-1}$, which is two orders of magnitude larger than the experimental measurements [38,39].

Furthermore, the anomalous Hall conductivity of $Mn_3Pt_{1-c}Ir_c$ decreases very quickly when increasing the concentration (c) of impurities, as shown in Fig. 5(c). Because the anomalous Hall conductivity is obtained by $\sigma^{\mathrm{H}} = \Theta/\rho_{zz}$, the decrease of σ^{H} can be attributed to the decreasing anomalous Hall angle (Θ) and the increasing longitudinal resistivity (ρ_{zz}), as shown in Figs. 5(a) and 5(b), respectively. We also notice that the anomalous Hall angle is

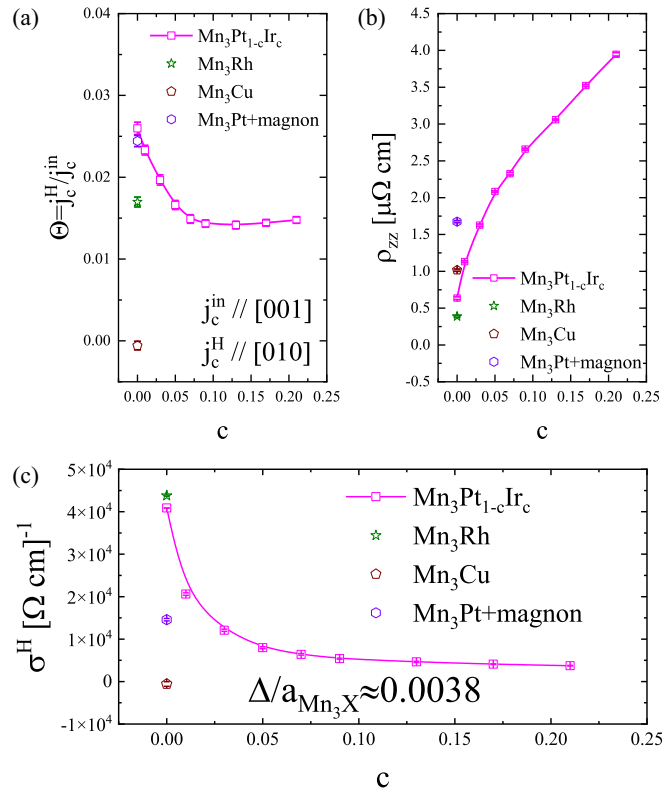

FIG. 5. (a) The anomalous Hall angle, (b) longitudinal resistivity, and (c) anomalous Hall conductivity of Mn_3X with X = Pt, Rh, Cu, and $Pt_{1-c}Ir_c$, respectively. Here, the root mean square of the phonon-induced atomic displacements is fixed by a value of $\Delta/a_{Mn_3X} \simeq 0.0038$, and the injected current and Hall current are in [001] and [010], accordingly.

more stable (twice change at maximum) than the longitudinal resistivity (one order of magnitude change) to the change in the impurity concentration (c). Therefore, if the resistivity was much larger in experiments, the measured anomalous Hall conductivity should be even smaller. Considering the polycrystal, grain boundary, surface roughness, and other impurities induced in the growth of the thin films in experiments, it should be much easier to obtain a much larger resistivity. For example, in a recent experiment on a 25-nm thin film of Mn_3Pt at 100 K [38], the measured longitudinal resistivity is about $\rho_{\mathrm{expt}} \simeq 160\ \mu\Omega\,\mathrm{cm}$ and the corresponding anomalous Hall conductivity is about $\sigma^{\mathrm{H}}_{\mathrm{expt}} \simeq 29\ (\Omega\,\mathrm{cm})^{-1}$. Another individual experiment on a 24-nm thin film of Mn_3Pt at room temperature [39] reports $\rho_{\mathrm{expt}} \simeq 120\ \mu\Omega\,\mathrm{cm}$ and $\sigma^{\mathrm{H}}_{\mathrm{expt}} \simeq 102\ (\Omega\,\mathrm{cm})^{-1}$. In this sense, if we use the anomalous Hall angle from our calculations, $\Theta \simeq 0.014$–0.026 as shown in Fig. 5(a), and the resistivity from the experiments, the anomalous Hall conductivity will be $\sigma^{\mathrm{H}} = \Theta/\rho_{\mathrm{expt}} \simeq 88 \sim 217\ (\Omega\,\mathrm{cm})^{-1}$, which is in the same order of magnitude of the above experimental measurements. Thus, the quality of the thin film should be the key to obtain this giant anomalous Hall effect and the huge resistivity is the reason that this giant anomalous Hall effect was not measured in previous experiments [29,32,34–39].

In conclusion, based on our first-principles approach, we study the anomalous Hall effect in noncollinear

antiferromagnetic $L1_2$-type Mn_3X (X = Ir, Pt, Rh) and find a remarkably large anomalous Hall conductivity, which is two orders of magnitude larger than that from Berry curvature calculations. By analyzing the scaling law of the anomalous Hall conductivity, we conclude that the TCS contribution is the physical origin of this giant anomalous Hall conductivity and dominates the anomalous Hall effect in $L1_2$-type Mn_3X-like materials. Moreover, when introducing impurities, we find that compared to the longitudinal resistivity, the anomalous Hall angle is more stable to the changing of impurity concentration, thus the anomalous Hall conductivity is strongly dependent on the longitudinal resistivity of the thin films. In this sense, a high-quality single-crystal thin film is necessary to obtain this giant anomalous Hall effect in experimental measurements in the future.

This work was financially supported by the National Key R&D Program of China (Grant No. 2021YFA1202200) and China Postdoctoral Science Foundation (Grant No. 2021T140549). K.X. is supported by the National Natural Science Foundation of China (Grant No. 11734004).

[1] E. H. Hall, Proc. Phys. Soc., London **4**, 325 (1880).
[2] R. Karplus and J. M. Luttinger, Phys. Rev. **95**, 1154 (1954).
[3] T. Jungwirth, Q. Niu, and A. H. MacDonald, Phys. Rev. Lett. **88**, 207208 (2002).
[4] N. Nagaosa, J. Sinova, S. Onoda, A. H. MacDonald, and N. P. Ong, Rev. Mod. Phys. **82**, 1539 (2010).
[5] J. Kondo, Prog. Theor. Phys. **27**, 772 (1962).
[6] Y. Yao, L. Kleinman, A. H. MacDonald, J. Sinova, T. Jungwirth, D.-s. Wang, E. Wang, and Q. Niu, Phys. Rev. Lett. **92**, 037204 (2004).
[7] Z. Fang, N. Nagaosa, K. S. Takahashi, A. Asamitsu, R. Mathieu, T. Ogasawara, H. Yamada, M. Kawasaki, Y. Tokura, and K. Terakura, Science **302**, 92 (2003).
[8] H. Toyosaki, T. Fukumura, Y. Yamada, K. Nakajima, T. Chikyow, T. Hasegawa, H. Koinuma, and M. Kawasaki, Nat. Mater. **3**, 221 (2004).
[9] S. R. Shinde, S. B. Ogale, J. S. Higgins, H. Zheng, A. J. Millis, V. N. Kulkarni, R. Ramesh, R. L. Greene, and T. Venkatesan, Phys. Rev. Lett. **92**, 166601 (2004).
[10] T. Miyasato, N. Abe, T. Fujii, A. Asamitsu, S. Onoda, Y. Onose, N. Nagaosa, and Y. Tokura, Phys. Rev. Lett. **99**, 086602 (2007).
[11] L. Wang, X. R. Wang, T. Min, and K. Xia, Phys. Rev. B **99**, 224416 (2019).
[12] D. Hou, G. Su, Y. Tian, X. Jin, S. A. Yang, and Q. Niu, Phys. Rev. Lett. **114**, 217203 (2015).
[13] L. Ye, Y. Tian, X. Jin, and D. Xiao, Phys. Rev. B **85**, 220403(R) (2012).
[14] L. Wang, T. Min, and K. Xia, Phys. Rev. B **103**, 054204 (2021).
[15] P. Nozières and C. Lewiner, J. Phys. France **34**, 901 (1973).
[16] S. Y. Liu, N. J. M. Horing, and X. L. Lei, Phys. Rev. B **74**, 165316 (2006).
[17] P. Łazarczyk, T. Story, A. Jędrzejczak, R. R. Gałązka, W. Mac, M. Herbich, and A. Stachow-Wójcik, J. Magn. Magn. Mater. **176**, 233 (1997).
[18] A. Crépieux and P. Bruno, Phys. Rev. B **64**, 014416 (2001).
[19] J. Smit, Physica **21**, 877 (1955).
[20] J. Smit, Physica **24**, 39 (1958).
[21] L. Berger, Phys. Rev. B **2**, 4559 (1970).
[22] T. Jungwirth, X. Marti, P. Wadley, and J. Wunderlich, Nat. Nanotechnol. **11**, 231 (2016).
[23] T. Jungwirth, J. Sinova, A. Manchon, X. Marti, J. Wunderlich, and C. Felser, Nat. Phys. **14**, 200 (2018).
[24] V. Baltz, A. Manchon, M. Tsoi, T. Moriyama, T. Ono, and Y. Tserkovnyak, Rev. Mod. Phys. **90**, 015005 (2018).
[25] H. Chen, Q. Niu, and A. H. MacDonald, Phys. Rev. Lett. **112**, 017205 (2014).
[26] Y. Zhang, Y. Sun, H. Yang, J. Železný, S. P. P. Parkin, C. Felser, and B. Yan, Phys. Rev. B **95**, 075128 (2017).
[27] T. Suzuki, R. Chisnell, A. Devarakonda, Y.-T. Liu, W. Feng, D. Xiao, J. Lynn, and J. Checkelsky, Nat. Phys. **12**, 1119 (2016).
[28] R. Shindou and N. Nagaosa, Phys. Rev. Lett. **87**, 116801 (2001).
[29] N. Kiyohara, T. Tomita, and S. Nakatsuji, Phys. Rev. Appl. **5**, 064009 (2016).
[30] J. Kübler and C. Felser, Europhys. Lett. **108**, 67001 (2014).
[31] L. Wang, K. Shen, S. S. Tsirkin, T. Min, and K. Xia, Appl. Phys. Lett. **120**, 012403 (2022).
[32] N. An, M. Tang, S. Hu, H. Yang, W. Fan, S. Zhou, and X. Qiu, Sci. China: Phys., Mech. Astron. **63**, 297511 (2020).
[33] C. Singh, V. Singh, G. Pradhan, V. Srihari, H. K. Poswal, R. Nath, A. K. Nandy, and A. K. Nayak, Phys. Rev. Res. **2**, 043366 (2020).
[34] T. Matsuda, N. Kanda, T. Higo, N. Armitage, S. Nakatsuji, and R. Matsunaga, Nat. Commun. **11**, 909 (2020).
[35] H. Iwaki, M. Kimata, T. Ikebuchi, Y. Kobayashi, K. Oda, Y. Shiota, T. Ono, and T. Moriyama, Appl. Phys. Lett. **116**, 022408 (2020).
[36] H. Bai, W. Zhu, Y. You, X. Chen, X. Zhou, F. Pan, and C. Song, Appl. Phys. Lett. **117**, 052404 (2020).
[37] W. Afzal, Z. Yue, Z. Li, M. Fuhrer, and X. Wang, J. Phys. Chem. Solids **161**, 110489 (2022).
[38] J. Mukherjee, T. S. Suraj, H. Basumatary, K. Sethupathi, and K. V. Raman, Phys. Rev. Mater. **5**, 014201 (2021).
[39] Z. Zhao, K. Zhang, Q. Guo, and Y. Jiang, Phys. E **138**, 115141 (2022).
[40] T. Ando, Phys. Rev. B **44**, 8017 (1991).
[41] O. K. Andersen, O. Jepsen, and G. Krier, in *Lectures on Methods of Electronic Structure Calculations - Proceedings of the Miniworkshop on Methods of Electronic Structure Calculations and Working Group on Disordered Alloys*, edited by V. Kumar, O. K. Andersen, and A. Mookerjee (World Scientific, Singapore, 1995), pp. 63–124.
[42] L. Vitos, *Computational Quantum Mechanics for Materials Engineers: The EMTO Method and Applications* (Springer, Berlin, 2007).
[43] Q. Zhang, J. Yan, Y. Zhang, and Y. Ke, Phys. Rev. B **100**, 075134 (2019).
[44] Z. Chen, Q. Zhang, Y. Zhang, L. Wang, M. Sang, and Y. Ke, Phys. Rev. B **102**, 035405 (2020).
[45] K. Xia, M. Zwierzycki, M. Talanana, P. J. Kelly, and G. E. W. Bauer, Phys. Rev. B **73**, 064420 (2006).
[46] A. A. Starikov, Y. Liu, Z. Yuan, and P. J. Kelly, Phys. Rev. B **97**, 214415 (2018).

[47] I. Turek, J. Kudrnovský, V. Drchal, L. Szunyogh, and P. Weinberger, Phys. Rev. B **65**, 125101 (2002).
[48] S. Wang, Y. Xu, and K. Xia, Phys. Rev. B **77**, 184430 (2008).
[49] L. Wang, R. J. H. Wesselink, Y. Liu, Z. Yuan, K. Xia, and P. J. Kelly, Phys. Rev. Lett. **116**, 196602 (2016).
[50] R. J. H. Wesselink, K. Gupta, Z. Yuan, and P. J. Kelly, Phys. Rev. B **99**, 144409 (2019).
[51] Y. Liu, A. A. Starikov, Z. Yuan, and P. J. Kelly, Phys. Rev. B **84**, 014412 (2011).
[52] Y.-N. Zhao, S.-X. Qu, and K. Xia, J. Appl. Phys. **110**, 064312 (2011).
[53] Y. Liu, Z. Yuan, R. J. H. Wesselink, A. A. Starikov, M. van Schilfgaarde, and P. J. Kelly, Phys. Rev. B **91**, 220405(R) (2015).
[54] R. Y. Umetsu, K. Fukamichi, and A. Sakuma, J. Phys. Soc. Jpn. **76**, 104712 (2007).
[55] J. Lin, S. Hsu, J. Lue, and P. Sheng, J. Phys. Chem. Solids **62**, 1813 (2001).